Electrical Power and Energy Systems 135 (2022) 107472

Contents lists available at ScienceDirect

International Journal of Electrical Power and Energy Systems

journal homepage: www.elsevier.com/locate/ijepes

Power oscillation suppression in multi-VSG grid with adaptive virtual inertia

Siqi Fu [a], Yao Sun [a,*], Zhangjie Liu [a], Xiaochao Hou [b], Hua Han [a], Mei Su [a]

[a] School of Automation, Central South University, Changsha, China
[b] Department of Electrical Engineering, Tsinghua University, Beijing, China

ARTICLE INFO

Keywords:
Distributed generation
Adaptive virtual inertia
Power oscillation
Virtual synchronous generators (VSGs)

ABSTRACT

Power oscillation is observed when a disturbance occurs in multiple virtual synchronous generators (VSGs) grid, potentially impacting the safe operation of the systems. This article proposes a distributed adaptive virtual inertia control method for suppressing the power oscillation and improving dynamic frequency response in the multiple VSGs grid. The basic principle of the method is that when the local frequency of a VSG deviates from the average frequency of its neighbors, the adaptive inertia control will exhibit a large inertia and when the local frequency starts to return, a small inertia is shaped to accelerate the convergence to the average frequency. The stability of the proposed algorithm is proved by the Lyapunov stability theory, and the guidelines on the key control parameters are provided. Finally, the simulation results and hardware-in-loop results demonstrate the effectiveness of the proposed control method.

1. Introduction

NOWADAYS, due to the aggravation of environmental pollution and energy crisis, the penetration of distributed generations (DGs) has been remarkably increased in the power system, leading to a dramatic change of modern power systems [1–3]. In particular, power system inertia provided by the rotating masses of synchronous generators (SG) decreases continuously. The reason is that most DGs, such as photovoltaic, wind, fuel cells, micro-turbine, and energy storage system (ESS), are connected to the grid by power electronics interfaces. The converter-based DGs have the characteristics of fast response and low inertia, compared with SG [4–6]. However, high power system inertia is generally desired as it can slow down the extremely large rate of change of frequency (RoCoF) and reduce frequency deviations, which effectively avoid undesirable load-shedding or massive blackouts [7–9].

To overcome these problems above, emulating virtual inertia has been introduced in the literature to imitate the synchronous generator (SG) operation as a virtual synchronous generator (VSG) [10,11]. The energy storage part of VSGs emulates the kinetic energy of SGs to support the islanded networks to maintain grid frequency in sudden load changes [12–14]. As expected, VSGs will be one of the leading components of the future advanced networks [15,16], Therefore, improving the stability of multi-VSG grids seems to be essential.

The introduction of the swing equation of VSG increases the order of the system. As a result, the inverter is prone to power oscillation during the transient process [17–36]. The research on the power oscillation of VSG has been primarily focused on a single VSG connected to an infinite bus. A small-signal model of the VSG was established in [17,18], where the influence of damping and inertia coefficients on power oscillation are studied. In [19–21], methods by adjusting the value of the damp coefficient adaptively are presented, in which the frequency oscillations are limited to a reliable range and output power oscillation is also weakened. [22] investigates adequately how the VSG affects low frequency oscillations (LFOs) in power systems and provides parameter design guidelines that effectively suppress LFO. Moreover, a bang-bang control approach [23,24] and a fuzzy-based control method [25] are proposed to improve dynamic frequency response, in which the inertia coefficient of VSG changes based on the real-time dynamics of angular speed. Subsequently, improved adaptive virtual inertia control methods with detailed parameter design guideline are proposed in [26,27]. In all of the power oscillation analysis mentioned above, only a single VSG case was considered.

The problem of the power oscillation of multi-VSG grid is more prominent and complex [28–36]. To enhance the transient stability of the system with multiple VSG units, particle swarm optimization is implemented to tune the parameters [28]. A parameter alternating VSG

* Corresponding author.
E-mail address: yaosuncsu@gmail.com (Y. Sun).

https://doi.org/10.1016/j.ijepes.2021.107472
Received 13 August 2020; Received in revised form 2 November 2020; Accepted 28 July 2021
Available online 20 August 2021

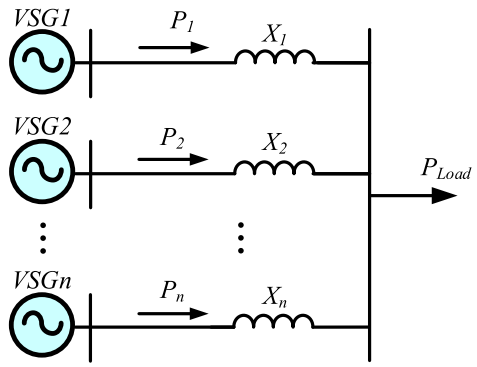

Fig. 1. The *n-VSG* electrical system.

controller is proposed to improve the damping performance to LFO modes and mitigate the negative impact of VSG on dc voltage stability in voltage source converter-based multi-terminal direct current systems [29]. However, analysis on interactions between different VSGs and power oscillation excitation mechanisms were not covered. Later, power oscillation excitation for two-parallel-VSG system with highly inductive line impedance has been analyzed in [30–32]. Further, [33] considers the influence of line resistance on power oscillation. Refs. [34] have explored parameter design criterion of *n*-parallel-VSG system. However, the design criterion conclusion is limited only to the single bus system and does not apply to complex network structure. Besides, the design criterion is considered to be extremely restrictive to be practical. Moreover, [35,36] adjust the power correction term in real-time by comparing the local frequency with the center of inertia (COI) of the frequency that effectively suppresses the power oscillation. However, the frequency derivative needs to be acquired that introducing high-frequency noise. Besides, they require communication networks with high-bandwidth communication links and a high level of connectivity that results in poor reliability.

To overcome the disadvantages of the methods in [35,36], we propose a new control method to suppress power oscillation of a multi-VSG grid by adjusting the inertia coefficient flexibly. The contributions of the paper can be summed up as:

(1) A distributed adaptive virtual inertia method is proposed to suppress the power oscillation. The adaptive term helps improve frequency dynamic response performance, and thus suppress power oscillation effectively. Compared with [35,36], it does not need to detect the frequency derivative, which could avoid the high-frequency noises due to the differential operator. Besides, it avoids centralized communication that reduces economic costs.
(2) Stability proof and detailed design guidelines are provided. In this work, the stability of the proposed nonlinear control algorithm is analyzed by the Lyapunov stability theory, and guideline for designing adaptive coefficient is presented.

The rest of the paper is organized as follows: Section II analyzes the active power oscillation phenomenon between multi-VSG under small disturbance. Section III introduces the proposed method. The Lyapunov stability analysis is investigated in Section IV. Simulation results and hardware-in-loop (HIL) results are provided in Section V and Section VI, respectively. Section VII concludes the paper.

2. Analysis of power oscillation of multi VSG

2.1. Basic VSG control scheme

The basic electromechanical swing equation of the i^{th} VSG is defined as:

$$J_i\omega^*\frac{d\omega_i}{dt} = P^* - P_i - D_i\omega^*(\omega_i - \omega^*) \tag{1}$$

where ω_i represents the virtual angular frequency of the i^{th} VSG, ω^* is the nominal angular frequency. P^* and P_i represents the active power reference and output power of the i^{th} inverter, respectively. J_i is the inertia coefficient and D_i is the damping coefficient.

The voltage regulation in the VSG system is achieved through the *Q–V* droop control so that the inverter has the primary voltage regulation characteristic. It is described as

$$V_i = V^* + n_i(Q^* - Q_i) \tag{2}$$

where V^* are the reference voltage amplitudes of the VSG, n_i is the droop coefficient, Q^* and Q_i are the reference and output reactive powers, respectively.

2.2. Power oscillation problem in Multi-VSG

To analyze the power oscillation problem in Multi-VSG, transfer function models for multiple VSG-based inverters will be established to analyze the related dynamic response characteristics.

For simplicity, assume that the line impedance is mainly inductive (if not, the virtual impedance is introduced), so that the active power and the reactive power of the VSG are approximately decoupled. In Fig. 1, the small-signal model of the power transfer equation of i^{th} VSG is

$$\Delta P_i = \frac{V_i V_{pcc}}{X_i} cos\delta_{i0}\Delta\delta_i \;=\; y_i\Delta\delta_i \tag{3}$$

where X_i is the total reactance, V_i is the amplitude of inverter output voltage, V_{pcc} is the amplitude of PCC voltage, δ_i is the phase difference between the inverter and PCC. Phase difference variation $\Delta\delta_i$ can be obtained as

$$\Delta\delta_i \;=\; \frac{1}{s}\left(\Delta\omega_i - \Delta\omega_g\right) \tag{4}$$

where $\Delta\omega_g$ represents the angular frequency variation of PCC.

Thus, the small-signal model of (1) can be expressed as

$$\frac{d\Delta\omega_i}{dt} = \frac{-y_i\Delta\delta_i - D_i\omega^*\Delta\omega_i}{J_i\omega^*} \tag{5}$$

In case of load change of ΔP_{Load}, it can be obtained that

$$\sum_{i=1}^{n}\Delta P_i = \Delta P_{Load} \tag{6}$$

Then the transfer function model can be obtained according to (3)-(6)

$$G(s) = \frac{\Delta P_i}{\Delta P_{Load}} = \frac{G_i(J_i\omega^* s + D_i\omega^*)}{\sum_{m=1}^{n} G_m(J_m\omega^* s + D_m\omega^*)} \tag{7}$$

$$G_i = \frac{y_i}{J_i\omega^* s^2 + D_i\omega^* s + y_i} \tag{8}$$

where *G(s)* represents the influence of load on the output power of the i^{th} inverter. Obviously, the output power of each paralleled VSG-based inverter is not only related to the load demand, but also affected by the parameters of other inverters as (7) shows. By analyzing *G(s)*, it is found that if the parameters satisfy the following relations

$$\begin{aligned} J_1 : J_2 : \cdots : J_n &= D_1 : D_2 : \cdots : D_n \\ &= \frac{1}{X_1} : \frac{1}{X_2} : \cdots : \frac{1}{X_n} \end{aligned} \tag{9}$$

G(s) will become a proportional component [34]. When load demand changes, the inverter's output power will change proportionally without an oscillation process. The conclusion (9) can be regarded as a constraint for parameter design. However, the constraint is too strict to

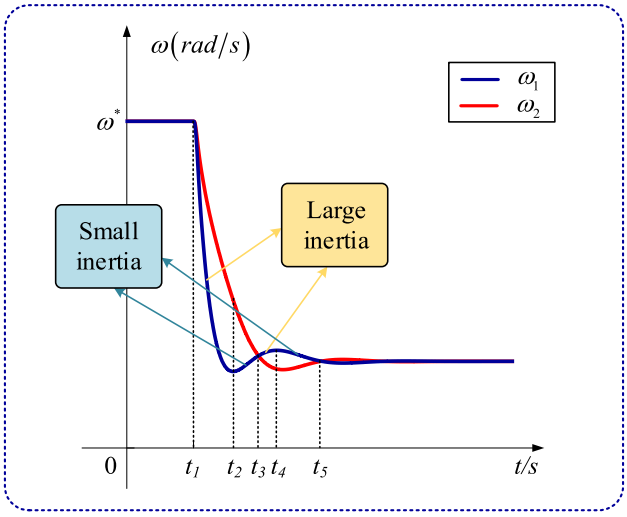

Fig.2. Oscillating curve of the rotor angular frequency.

Table 1
Design Principle of Virtual Inertia.

Frequency deviation	Change rate $d\omega_i/dt$	J change
$\omega_i < \omega_j$	<0	increase
$\omega_i < \omega_j$	>0	decrease
$\omega_i > \omega_j$	>0	increase
$\omega_i > \omega_j$	<0	decrease

be practical. To relax the constraint, the mechanisms for power oscillation were analyzed in [33]. At the moment of load changes, the angular velocity of VSG cannot change abruptly and will maintain its original. Thus,

$$\frac{\dot{\omega}_i}{\dot{\omega}_j} \approx \frac{\Delta P_i}{J_i \omega^*} \frac{J_j \omega^*}{\Delta P_j} \approx \frac{X_i}{X_j} \frac{J_j}{J_i} \tag{10}$$

Further, loose constraint can be expressed as

$$J_1 : J_2 : \cdots : J_n = \frac{1}{X_1} : \frac{1}{X_2} : \cdots : \frac{1}{X_n} \tag{11}$$

From (10), the different angular accelerations are considered as the initial system oscillation excitation. Thus, if the angular acceleration of each VSG is exactly equal, the initial system oscillation excitation will be zero. Otherwise, different angular accelerations will directly cause periodical power angle oscillation and active power oscillation between different inverters.

3. Proposed adaptive virtual inertia

3.1. Proposed adaptive virtual inertia

From (5) and (10), it can be found that adjusting inertia coefficient dynamically is a direct way to change the angular acceleration and reduce the oscillation. Based on this idea, we present an adaptive virtual inertia control to solve the problem of the power oscillation.

To describe clearly the principle of the proposed algorithm, the frequency dynamic response of the two-VSG system is shown in Fig. 2. A disturbance on the load is put at t_1. As shown in Fig. 2, the typical oscillation process is divided into four situations, and the relationship between J and the angular velocity variation is analyzed. Since the angular velocity and power variation characteristics in each interval are different, the required rotor inertia is also different. Here, the variation trend of virtual inertia of VSG1 is mainly analyzed. The frequency ω_2 is taken as a static reference of ω_1. The VSG1 system should have a slow response when ω_1 deviates from ω_2, and thus large inertia should be adopted. On the other hand, small inertia should be adopted to accelerate system dynamics when ω_1 returns to ω_2. Thus, in the dynamic process, it is beneficial to promote the consistency of response curves of ω_1 and ω_2, so as to achieve the effect of suppressing frequency oscillation.

Based on the analysis above, the design principle of virtual inertia at different operation states applicable for multi-VSG system is obtained as shown in Table 1, where ω_i is local angular frequency of the i^{th} inverter and ω_j is the angular frequency of neighbors of the i^{th} inverter.

According to the design principle shown in Table 1, a concise and unified mathematical equation of the adaptive virtual inertia is constructed as follows

$$J_i = J_{0i} + k_i \sum_{j \in N_i} (\omega_i - \omega_j) \frac{d\omega_i}{dt} \tag{12}$$

where N_i represents the set of the neighbors of the i^{th} inverter. From (12), the constructed inertia has two terms. The first term J_{0i} is the nominal constant inertia, and the second term is the adaptive compensation inertia. k_i is a positive inertia compensation coefficient, which can adjust the response speed of the frequency dynamic. Actually, the adaptive virtual inertia algorithm considers ω_j as a reference value for real-time updates. The total moment of inertia is modified based on the relative angular velocity (ω_i-ω_j) and the change-rate of local angular frequency in real-time. Especially, in the nominal steady-state ($\omega_i = \omega_j$), the second term of adaptive compensation inertia would be 0, and the total inertia is equal to J_{0i}. Conventionally, the virtual inertia J is used to slow down the change rate of COI of frequency and thus raise the level of the overall inertia of the system. Here, the adaptive term only helps improve frequency dynamic performance and suppress the power oscillation but does not affect the total inertia of the system.

3.2. Practical control scheme without derivative action

In (12), it is worth noting that the adaptive inertia value would be inaccurate if we calculate it directly since the frequency derivative is sensitive to measurement noise [25,34–35]. Thus, we need to find a practical and effective method to address the issue.

Define the slip frequency ω_{si} as

$$\omega_{si} = \omega_i - \omega^* \tag{13}$$

where ω^* is the nominal angular frequency. Thus,

$$\omega_i - \omega_j = \omega_{si} - \omega_{sj} \tag{14}$$

Substituting the constructed inertia (12) into the typical VSG control (1) yields

$$\left(J_{0i} + k_i \sum_{j \in N_i} (\omega_{si} - \omega_{sj}) \frac{d\omega_{si}}{dt} \right) \frac{d\omega_{si}}{dt} = P^* - P_i - D_i \omega_{si}$$

where simplification is made since the ω^* multiplied by J and D is not the key parameter.

Rewriting (15) yields

$$k_i \sum_{j \in N_i} (\omega_{si} - \omega_{sj}) \dot{\omega}_{si}^2 + J_{0i} \dot{\omega}_{si} + D_i \omega_{si} = P_{res} \tag{16}$$

$$P_{res} = P^* - P_i \tag{17}$$

where P_{res} is the reserved power, which implies the difference between nominal power and actual output power.

Obviously, equation (16) is a quadratic equation in the variable $\dot{\omega}_s$. According to the Vieta Theorem, two roots are solved.

$$\dot{\omega}_{si} = \frac{-J_{0i} \pm \sqrt{J_{0i}^2 - 4k_i \sum_{j \in N_i} (\omega_{si} - \omega_{sj})(D_i \omega_{si} - P_{res})}}{2k_i \sum_{j \in N_i} (\omega_{si} - \omega_{sj})} \tag{18}$$

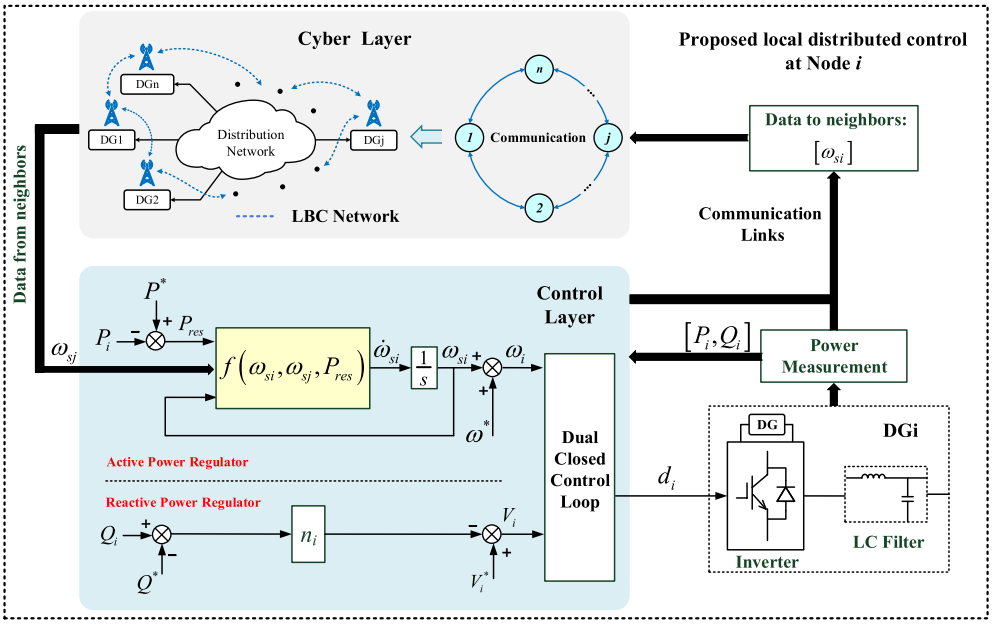

Fig.3. Schematic diagram of the proposed adaptive virtual inertia control algorithm.

As both $\dot{\omega}_{si}\sum_{j\in N_i}(\omega_{si}-\omega_{sj})>0$ and $\dot{\omega}_{si}\sum_{j\in N_i}(\omega_{si}-\omega_{sj})<0$ may exist in (18), only one root of (18) is effective, derived as follow

$$\begin{aligned}\dot{\omega}_{si} &= f(\omega_{si},\omega_{sj},P_{res})\\ &= \frac{-J_{0i}+\sqrt{J_{0i}^2-4k_i\sum_{j\in N_i}(\omega_{si}-\omega_{sj})(D_i\omega_{si}-P_{res})}}{2k_i\sum_{j\in N_i}(\omega_{si}-\omega_{sj})}\end{aligned} \tag{19}$$

To avoid the singular point (ω_{si}-$\omega_{sj}=0$), rewrite (19) by numerator rationalization

$$\begin{aligned}\dot{\omega}_{si} &= f(\omega_{si},\omega_{sj},P_{res})\\ &= \frac{-2(D_i\omega_{si}-P_{res})}{J_{0i}+\sqrt{J_{0i}^2-4k_i\sum_{j\in N_i}(\omega_{si}-\omega_{sj})(D_i\omega_{si}-P_{res})}}\end{aligned} \tag{20}$$

Then, the improved active power-frequency (P-ω) control based on the adaptive virtual inertia algorithm is obtained by combining (13) and (20).

$$\omega_i=\omega^*+\omega_{si} = \omega^*+\int f(\omega_{si},\omega_{sj},P_{res})dt \tag{21}$$

From (21), the angular frequency reference is a function of output active power and the angular frequency of neighbors. The detailed control scheme with adaptive virtual inertia is presented in Fig. 3. The control input is the real-time active power and the angular frequency of neighbors. The control output is the angular frequency reference. The control function (21) is derived from (12)-(15), and its design principle is shown in Table 1. Compared with the power loop of a typical VSG, the control algorithm with adaptive virtual inertia is added. It is worth noting that the frequency derivative term is avoided in Fig. 3. Thus, the proposed control scheme is simple and practical.

3.3. Design guideline for compensation coefficient

In this subsection, the design guidelines for key control parameters, such as the damping coefficient D_i, the initial inertia coefficient J_0 and the compensation coefficient k_i are discussed.

The system angular frequency should lie in the allowable range $[\omega_{min}, \omega_{max}]$. Thus, the specific design of damping coefficient D is as follows:

$$D_i\geqslant\frac{P_{max}-P_{min}}{\omega_{max}-\omega_{min}} \tag{22}$$

In the steady state, the adaptive inertia term would be 0, and the total inertia J is equal to J_0. Thus, adaptive terms are not considered when designing initial inertia coefficient J_0. The dynamic of the nominal steady-state is obtained from (15)

$$J_{0i}\ddot{\delta}_i + D_i\dot{\delta}_i + \frac{V_iV^*}{X_i}sin\delta_i=P^* \tag{23}$$

Linearization of (23) at the steady-state point yields

$$J_{0i}\Delta\ddot{\delta}_i + D_i\Delta\dot{\delta}_i + \frac{V_iV^*cos\delta_{i0}}{X_i}\Delta\delta_i=0 \tag{24}$$

The natural frequency ω_n and damping ratio ζ are obtained as

$$\omega_n=\sqrt{\frac{V_iV^*cos\delta_{i0}}{J_0X_i}};\ \zeta=\frac{D_i}{2}\sqrt{\frac{X_i}{J_0V_iV^*cos\delta_{i0}}} \tag{25}$$

The damping factor $\zeta\in[0.1, 1.414]$ should be met to get a satisfactory transient response [37]. The initial inertia coefficient J_0 should be chosen as

$$\frac{0.125D_i^2X_i}{(V^*)^2}\leqslant J_{0i}=\frac{D_i^2X_i}{4\zeta^2V_iV^*cos\delta_{i0}}\leqslant\frac{25D_i^2X_i}{(V^*)^2} \tag{26}$$

The more detailed design of the damping coefficient and the initial inertia coefficient can be seen in [26]. In this paper, the inertia compensation coefficient k_i is mainly discussed. In (19), the angular acceleration $\dot{\omega}_s$ must be a real number rather than an imaginary number to ensure the validity of the proposed control. Hence, the following condition must hold identically.

$$J_{0i}^2-4k_i\sum_{j\in N_i}(\omega_{si}-\omega_{sj})(D_i\omega_{si}-P_{res})\geqslant0 \tag{27}$$

Thus,

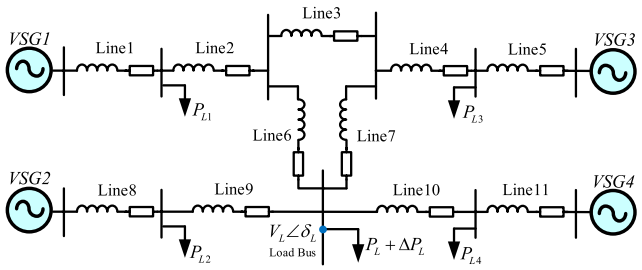

Fig. 4. The four-VSG simulated test system.

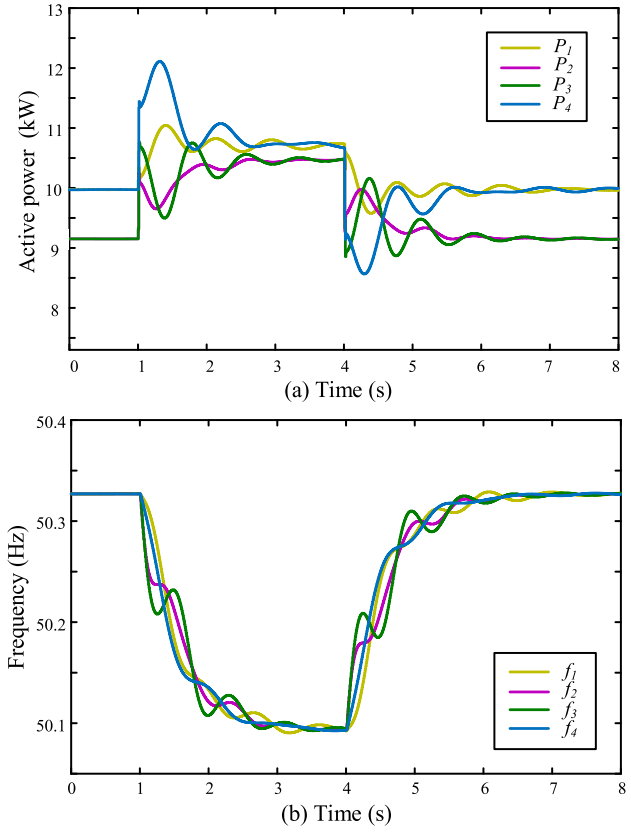

Fig. 5. output active powers (a) and system frequency (b) of the system with a constant inertia coefficient.

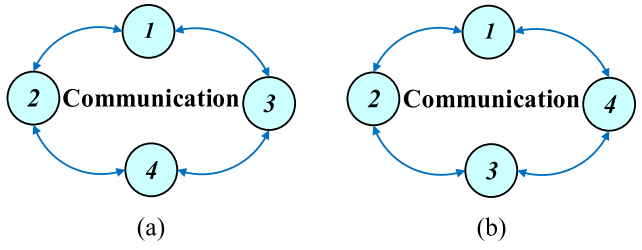

Fig. 6. communication topology (a) and communication topology (b).

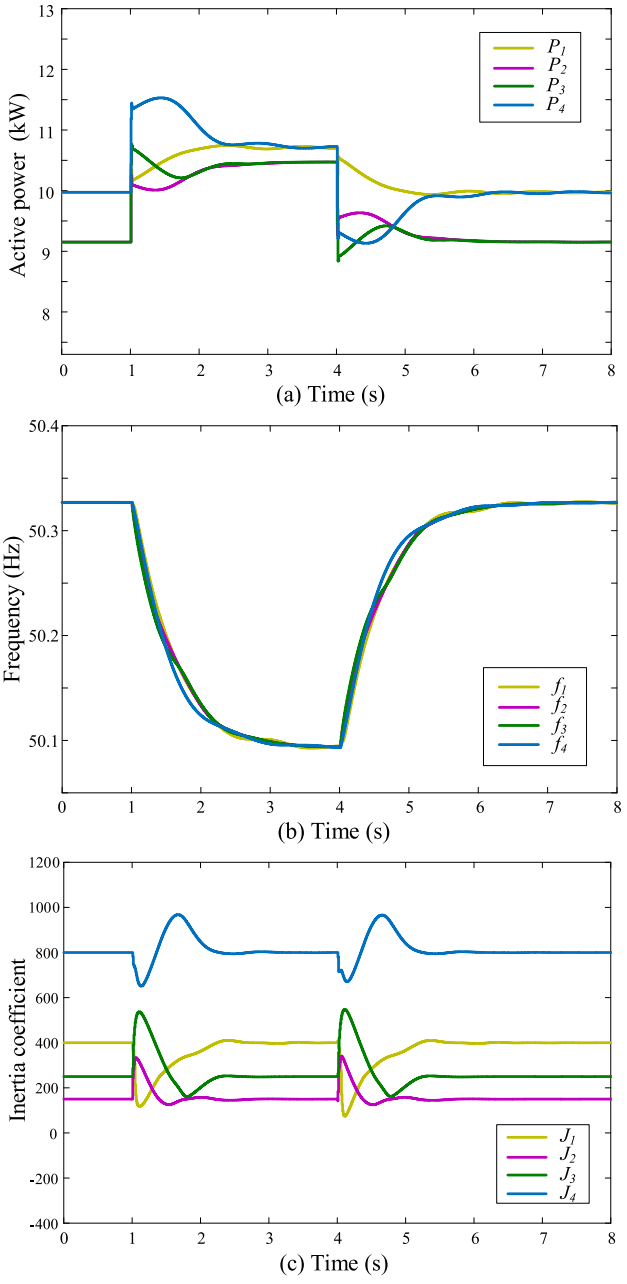

Fig. 7. Output active powers (a), system frequency (b), and the variation trend of total inertia coefficient (c) of the system with $k_i = 1000$ under communication topology (a).

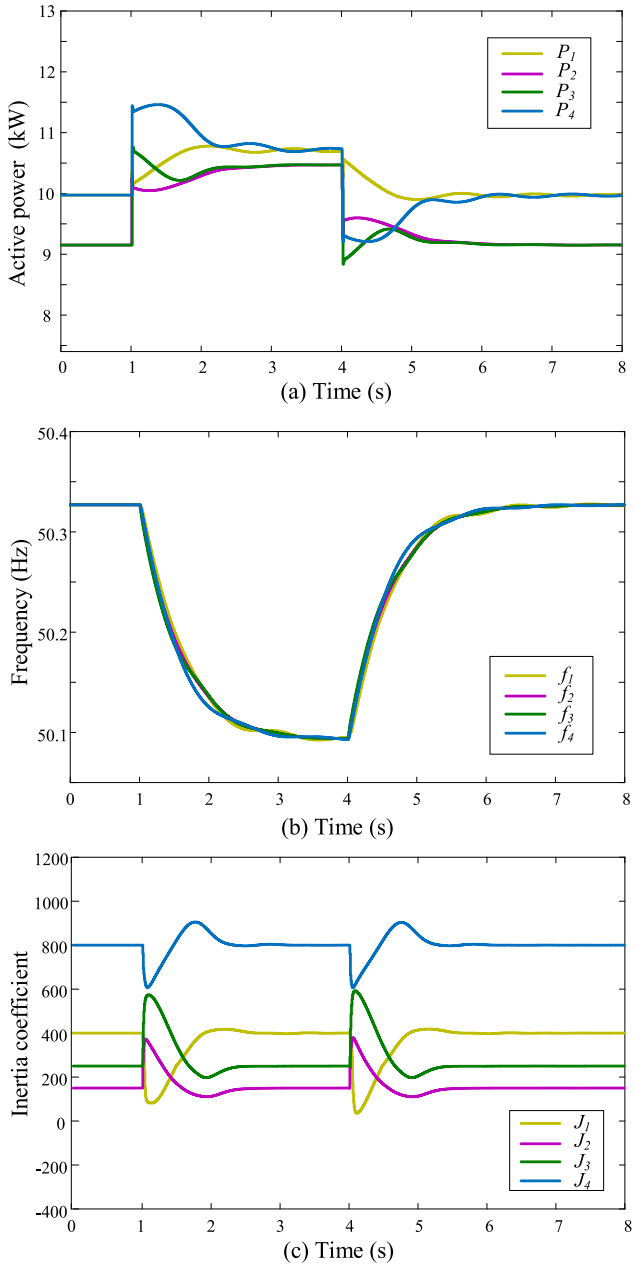

Fig. 8. Output active powers (a), system frequency (b), and the variation trend of total inertia coefficient (c) of the system with $k_i = 1000$ under communication topology (b).

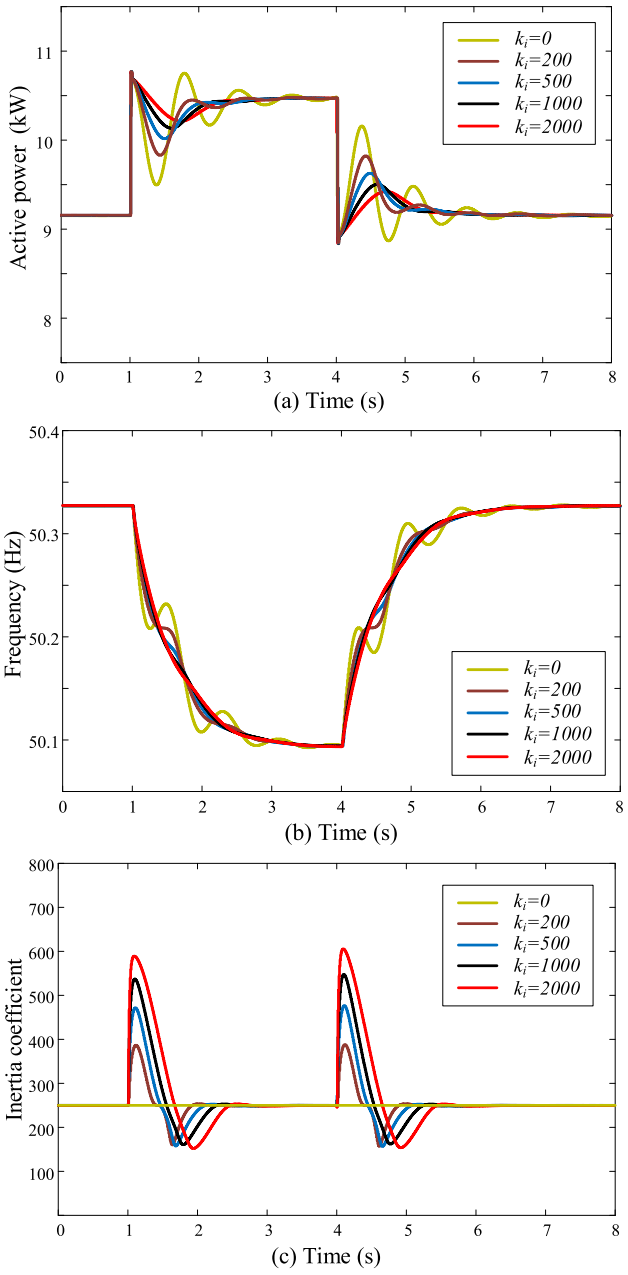

Fig. 9. Output active power (a), system frequency (b), and the variation trend of total inertia coefficient (c) of the system with different adaptive virtual inertia coefficient (k_i).

$$\begin{cases} J_{0i}^2 \geqslant 4k_i \sum_{j\in N_i}(\omega_{si}-\omega_{sj})(D_i\omega_{si}-P_{res});\ when \\ \omega_{si}=\omega^*-\omega_{max};\ P_{res}=P^*-P_{min};\ \sum_{j\in N_i}(\omega_{si}-\omega_{sj})=\sum_{j\in N_i}(\omega_{min}-\omega_{max}); \\ J_{0i}^2 \geqslant 4k_i \sum_{j\in N_i}(\omega_{si}-\omega_{sj})(D_i\omega_{si}-P_{res});\ when \\ \omega_{si}=\omega^*-\omega_{min};\ P_{res}=P^*-P_{max};\ \sum_{j\in N_i}(\omega_{si}-\omega_{sj})=\sum_{j\in N_i}(\omega_{max}-\omega_{min}); \end{cases} \tag{28}$$

In the steady-state as shown in (15), there exists

$$\begin{cases} P^*-P_{min} = -D(\omega^*-\omega_{max}) \\ P^*-P_{max} = -D(\omega^*-\omega_{min}) \end{cases} \tag{29}$$

Combining (28) and (29), the range of the inertia compensation coefficient k_i is given by

$$0 \leqslant k_i \leqslant \frac{J_{0i}^2}{8E} \tag{30}$$

where

$$E = max\left\{\sum_{j\in N_i}(\omega_{min}-\omega_{max})(P_{min}-P^*), \sum_{j\in N_i}(\omega_{max}-\omega_{min})(P_{max}-P^*)\right\} \tag{31}$$

In (12), a relatively large value of compensation coefficient k_i is favorable to exhibit the effectiveness of adaptive inertia control. Thus, k_i should be chosen as an upper bound according to (30).

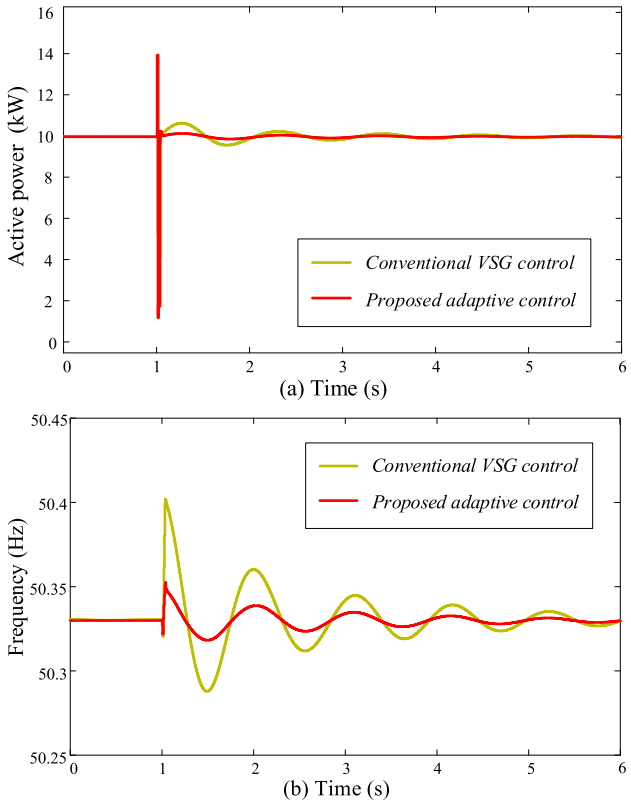

Fig. 10. Output active powers (a), system frequency (b) of VSG1 with conventional VSG control and proposed adaptive virtual inertia control under short-circuit fault.

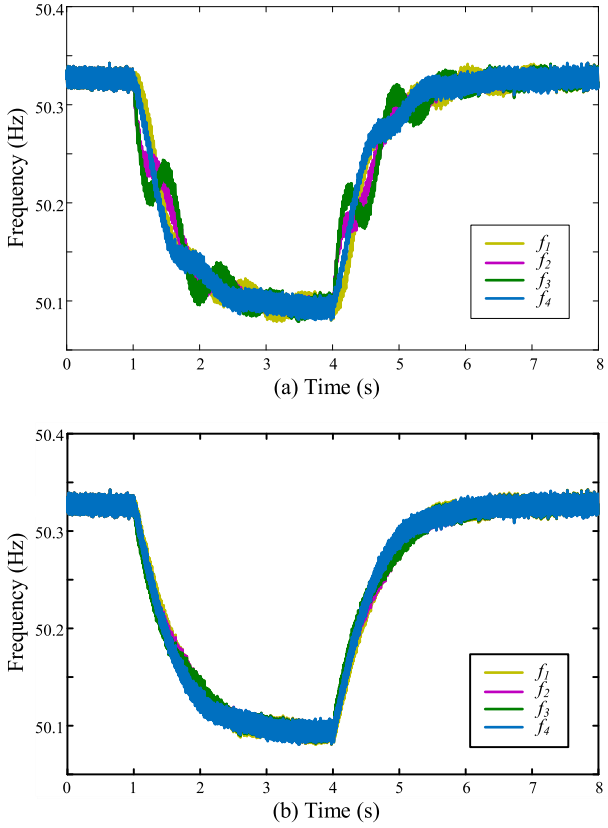

Fig. 11. System frequency without (a) and with (b) adaptive virtual inertia coefficient.

3.4. Stability analysis

The stability of the Multi-VSG under the proposed control algorithm will be investigated based on the Lyapunov stability theorem in this section.

I. Stability analysis without time delay

The network model of the multi-machine system is described by the nodal admittance equation. By eliminating the load nodes, the reduced network can be described as [37]

$$P_i = V_i^2 G_{ii} + \sum_{m\neq i}^{n} V_i V_m G_{im} cos(\delta_i - \delta_m) + \sum_{m\neq i}^{n} V_i V_m B_{im} sin(\delta_i - \delta_m) \tag{32}$$

where $\overrightarrow{V}_i = V_i e^{j\delta_i}$ is the voltage at node i, and $Y_{im} = G_{im} + jB_{im}$ are the elements of the reduced admittance matrix.

Simplifying (32) as

$$P_i = P_{0i} + \sum_{m\neq i}^{n} k_{im} sin(\delta_i - \delta_m) \tag{33}$$

where $k_{im} = V_i V_m B_{im}$ is the magnitude of the power–angle characteristic for the transfer equivalent branch and

$$P_{0i} = V_i^2 G_{ii} + \sum_{m\neq i}^{n} V_i V_m G_{im} cos(\delta_i - \delta_m) \tag{34}$$

Generally, P_{0i} depends on power angles and is not constant during the transient period when the rotors are swinging. Stability analysis of the multi-machine system by the Lyapunov direct method is straightforward assuming that P_{0i} is a constant. That assumption in practice means that transmission losses in transfer branches are assumed to be constant and added to the equivalent loads.

According to (15)-(16), the dynamic of the proposed control algorithm can be expressed as

$$k_i \sum_{j\in N_i} (\omega_{si} - \omega_{sj}) \left(\dot{\omega}_{si}\right)^2 + J_{0i}\dot{\omega}_{si} + D_i\omega_{si} = P^* - P_i \tag{35}$$

Let $\dot{\delta}_{si} = \omega_{si}$, the simplified multi-VSG grid model resulting from Equations (32) and (33) can be summarized in the following set of state-space equations:

$$\begin{aligned} k_i \sum_{j\in N_i} \left(\dot{\delta}_{si} - \dot{\delta}_{sj}\right) \left(\ddot{\delta}_{si}\right)^2 + J_{0i}\ddot{\delta}_{si} + D_i\dot{\delta}_{si} \\ = P^* - P_{0i} - \sum_{m=1,m\neq i}^{n} k_{im} sin(\delta_i - \delta_m) \end{aligned} \tag{36}$$

To introduce the Lyapunov function, in the first step, we need to define the potential and kinetic energy functions that are presented as:

$$\begin{cases} E_k = \dfrac{1}{2}\sum_{i=1}^{n} J_{0i}\omega_{si}^2 \\ E_p = -\sum_{i=1}^{n} \left(P_i^* - k_{ii}\right)\left(\delta_i - \delta_i^*\right) - \sum_{i=1}^{n-1}\sum_{m=i+1}^{n} k_{im}\left[cos\delta_{im} - cos\delta_{im}^*\right] \end{cases} \tag{37}$$

Now, the Lyapunov function is obtained as a sum of two energy functions:

$$V_1 = E_k + E_p \tag{38}$$

If $\delta_{im} < \frac{\pi}{2}$for all VSGs, energy function V_1 defined in (38) satisfies the condition of being a Lyapunov function that has been discussed in detail in [36,37]. The derivative of V_1 is expressed as

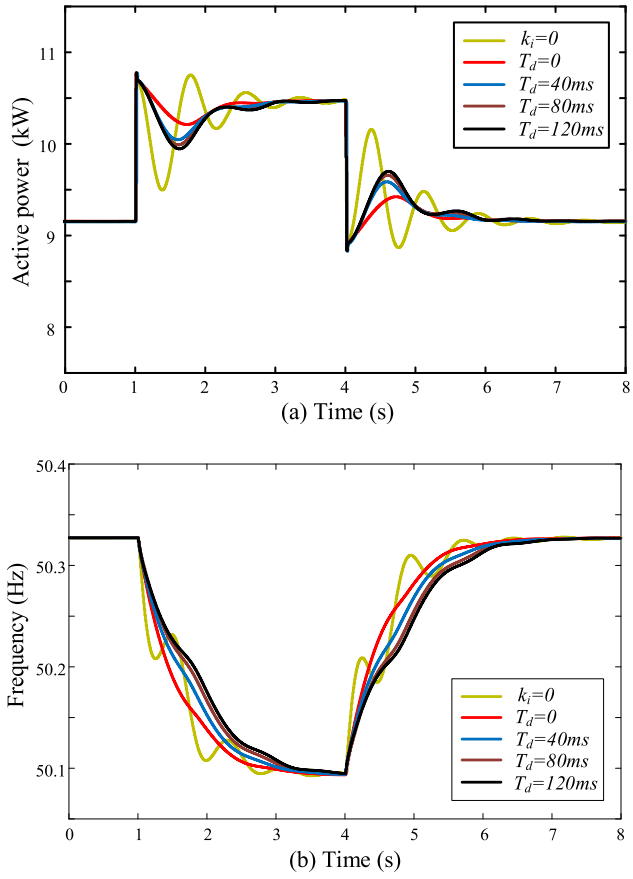

Fig. 12. Output active powers (a) and system frequency (b) of the system with adaptive virtual inertia method under different time delay.

$$\frac{dV_1}{dt} = -\sum_{i=1}^{n} D_i\dot{\delta}_i^2 - \sum_{i=1}^{n}\dot{\delta}_i k_i\ddot{\delta}_i^2\sum_{j\in\Omega}\left(\dot{\delta}_i - \dot{\delta}_j\right) \tag{39}$$

Thus,

$$\frac{dV_1}{dt} = -\dot{\delta}^T\left(D + \frac{1}{2}(KL + LK)\right)\dot{\delta} = -\dot{\delta}^T C\dot{\delta} \tag{40}$$

where L is a Laplace matrix that depends on the communication topology and

$$\begin{cases} \dot{\delta}^T = \left[\dot{\delta}_1, \dot{\delta}_2 \cdots \dot{\delta}_n\right]^T \\ D = diag\{D_1, D_2 \cdots D_n\} \\ K = diag\left\{k_1\ddot{\delta}_1^2, k_2\ddot{\delta}_2^2 \cdots k_n\ddot{\delta}_n^2\right\} \end{cases} \tag{41}$$

The next proof employs the following two lemmas:

Definition 1.. *Let A be a n × n matrix with complex or real elements with eigenvalues $\lambda_1,\ldots,\lambda_n$. Then the spectral radius $\rho(A)$ of A is $\rho(A) = \max_{1\leqslant i\leqslant n}|\lambda_i|$, i.e., the largest absolute value (or complex modulus) of its eigenvalues.*

Lemma 1.. *Let $A \in C^{n\times n}$ with spectral radius $\rho(A)$ and for any matrix norm $\|\bullet\|$, we have $\rho(A)\leqslant\|A\|$.*

Lemma 2.. *If $\lambda_1\leqslant\lambda_2\leqslant\cdots\leqslant\lambda_n$ are the eigenvalues of a real symmetric matrix A, and $\beta_1\leqslant\beta_2\leqslant\cdots\leqslant\beta_n$ are the eigenvalues of a real symmetric matrix B, we obtain*

$$\lambda_i + \beta_1 \leqslant \eta_i \leqslant \cdots \leqslant \lambda_i + \beta_n \tag{42}$$

where $\eta_1\leqslant\eta_2\leqslant\cdots\leqslant\eta_n$ are the eigenvalues of matrix $A + B$. (The proof is presented in [38])

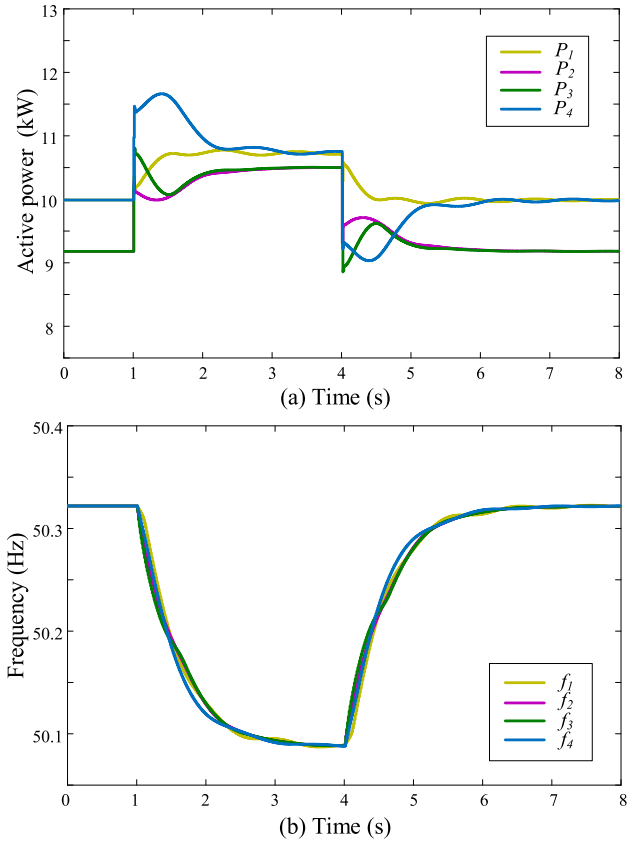

Fig. 13. System frequency without (a) and with (b) adaptive virtual inertia coefficient under single communication link failure.

Lemma 3.. *For a symmetric matrix $M = \begin{bmatrix} A & B \\ C & D \end{bmatrix}$, the following three conditions are equivalent.*

(1). *M* is a positive definite matrix.
(2). *A* and *D-CA*$^{-1}$*B* are both positive definite matrices.
(3). *D* and *A-BD*$^{-1}$*C* are both positive definite matrices.

Proof.. *According to Lemma* 1, *we have*

$$\rho\left(\frac{1}{2}(KL + LK)\right) \leqslant \left\|\frac{1}{2}(KL + LK)\right\| \leqslant \|K\|\|L\| \leqslant k_{max}\|L\| \tag{43}$$

where k_{max} represents the maximum elements of the diagonal matrix *K that is bounded due to a limiter unit.*

Further, designing the control parameter satisfying

$$k_{max}\|L\| < d_{min} \tag{44}$$

i.e.

$$\rho\left(\frac{1}{2}(KL + LK)\right) < d_{min} \tag{45}$$

where d_{min} represents the minimum damping coefficient. Thus, according to lemma 2

$$\lambda\left(D + \frac{1}{2}(KL + LK)\right) > 0 \tag{46}$$

i.e. the eigenvalues of the symmetric matrix *C* are positive. Combining (43)-(46) yields

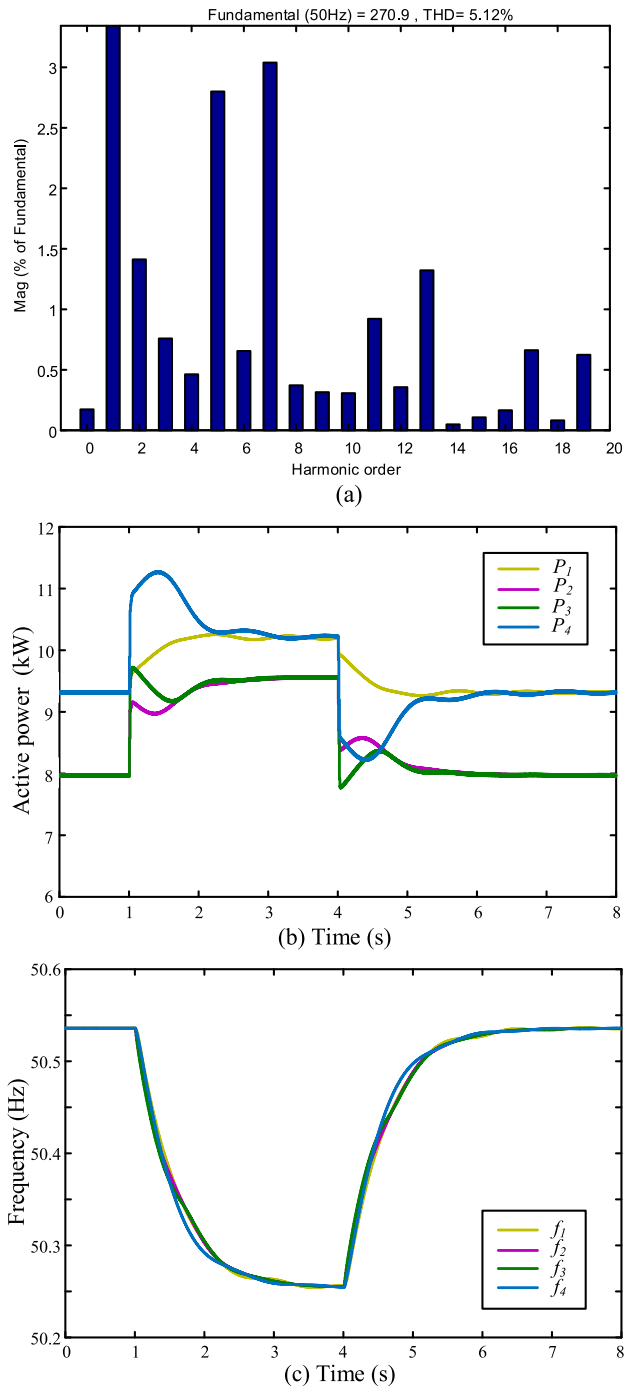

Fig. 14. Harmonic analysis of the load voltage (a), output active powers (b) and system frequency (c) of the system with the proposed method.

$$\frac{dV_1}{dt} = -\dot{\delta}^T C\dot{\delta} < 0 \tag{47}$$

Thus, the energy function of the system decreases over time. The stability of the system is proved.

3.5. Stability analysis with time delay

Considering positive time delay τ, the system model (36) can be expressed as

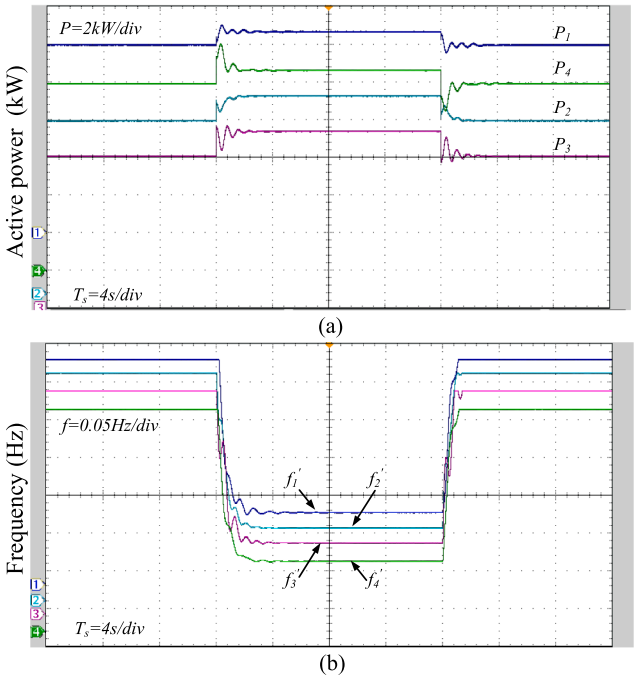

Fig. 15. output active powers (a) and system frequency (b) of the system with a constant inertia coefficient (c).

$$k_i\sum_{j\in N_i}\left(\dot{\delta}_{si}(t)-\dot{\delta}_{sj}(t-\tau)\right)\left(\ddot{\delta}_{si}(t)\right)^2 + J_{0i}\ddot{\delta}_{si}(t) + D_i\dot{\delta}_{si}(t) = P^* - P_{0i} - \sum_{m=1,m\neq i}^{n} k_{im}sin(\delta_i(t)-\delta_m(t)) \tag{48}$$

A Lyapunov function is reconstructed as

$$V = V_1 + V_2 \tag{49}$$

where $V_1 = E_k + E_p$ and $V_2 = \int_{t-\tau}^{t}\dot{\delta}^T(s)R\dot{\delta}(s)ds$. R is a random positive definite matrix.

Taking the time derivative of V gives that

$$\begin{cases} \dfrac{dV_1}{dt} = -\dot{\delta}^T D\dot{\delta} - \left[\dot{\delta}^T, \dot{\delta}_\tau^T\right]\begin{bmatrix} nK & \dfrac{K(L-nI)}{2} \\ \dfrac{(L-nI)K}{2} & 0 \end{bmatrix}\begin{bmatrix}\dot{\delta}\\ \dot{\delta}_\tau\end{bmatrix} \\ \dfrac{dV_2}{dt} = \dot{\delta}^T R\dot{\delta} - \dot{\delta}_\tau^T R\dot{\delta}_\tau \end{cases} \tag{50}$$

where I is an unit matrix. Thus,

$$\frac{dV}{dt} = -\left[\dot{\delta}^T, \dot{\delta}_\tau^T\right]\begin{bmatrix} D+nK-R & \dfrac{K(L-nI)}{2} \\ \dfrac{(L-nI)K}{2} & R \end{bmatrix}\begin{bmatrix}\dot{\delta}\\ \dot{\delta}_\tau\end{bmatrix} = -\left[\dot{\delta}^T, \dot{\delta}_\tau^T\right]Q\begin{bmatrix}\dot{\delta}\\ \dot{\delta}_\tau\end{bmatrix} \tag{51}$$

Theorem 1.. *The system (48) is asymptotically stable and the system stability is independent of time delay τ if there exist positive definite matrix R satisfying the inequality (52).*

$$\frac{1}{4}k_{max}^2\|L-nI\|^2\left\|R^{-1}\right\| < d_{min} - \varepsilon_{max} \tag{52}$$

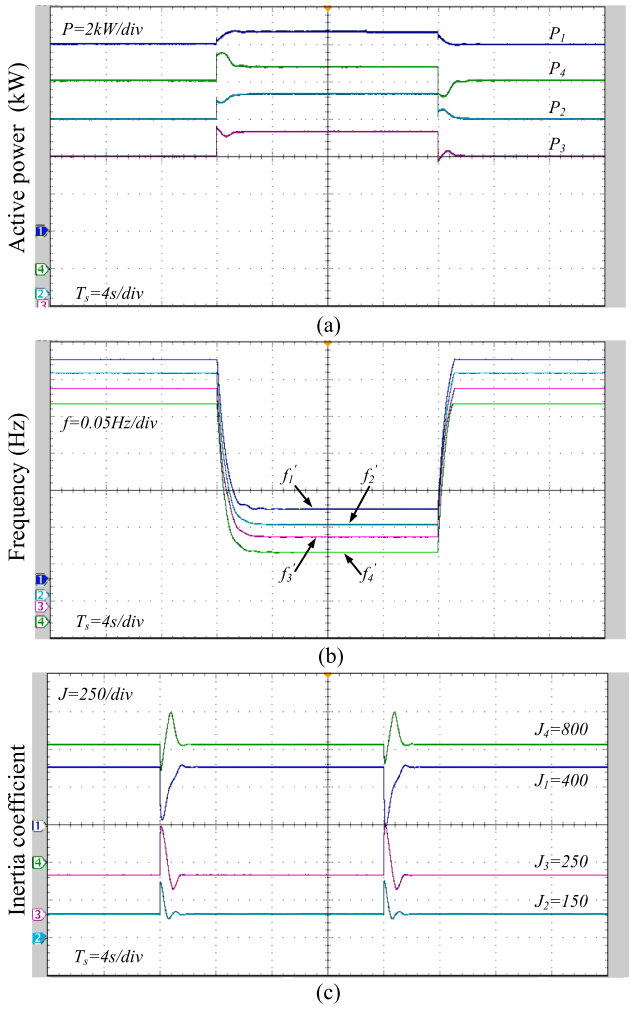

Fig. 16. Output active power (a), system frequency (b), and the variation trend of total inertia coefficient (c) of the system with the proposed method ($k_i = 1000$).

where ε_{max} represents the maximum eigenvalue of matrix R.

Proof.. *According to the compatibility of matrix norm*

$$\frac{1}{4}k_{max}^2\|(L-nI)\|^2\left\|R^{-1}\right\|\geqslant\|W\|\geqslant\rho(W) \tag{53}$$

where $W = \frac{K(L-nI)}{2}R^{-1}\frac{(L-nI)K}{2}$. According to Definition 1 and Lemma 2,

$$\begin{aligned}&\lambda[(D+nK-R)-W]\\ \geqslant& d_{min}-\varepsilon_{max}-\mu_{max}\geqslant d_{min}-\varepsilon_{max}-\rho(W)\end{aligned} \tag{54}$$

where μ_{max} represents the maximum eigenvalue of matrix W. Suppose that inequality (52) is satisfied. Then,

$$\lambda[(D+nK-R)-W]>0 \tag{55}$$

Thus, matrices R and $\left[(D+nK-R)-\frac{K(L-nI)}{2}R^{-1}\frac{(L-nI)K}{2}\right]$ are both positive definite matrices. According to Lemma 3, the symmetric matrix Q is positive. Thus, the energy function of the system decreases over time. The stability of the system is proved and is independent of time delay.

4. Simulation results

In this section, to validate the effectiveness of the proposed method, simulations have been carried out in Matlab/Simulink. The circuit of the

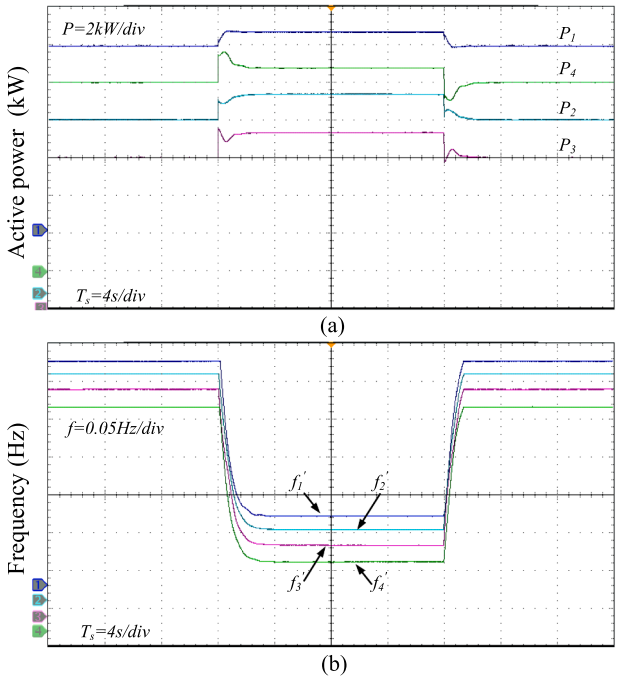

Fig. 17. Output active powers (a) and the frequency (b) of the system with the proposed method with time delay $T_d = 100$ *ms*.

Table 2
Parameters of the test system.

Line Parameters		
	Resistance (Ω)	Inductance (mH)
Line 1	0.8	12
Line 2	0.4	6
Line 3, Line 4, Line 6, Line 7, Line10	0.8	3
Line 5	0.5	1
Line 8	0.2	5
Line 9	0.2	3.5
Line 11	0.8	4
System Parameters		
Parameter	**Symbol**	**Value**
Nominal frequency	f^*	50HZ
Nominal voltage	V^*	380 V
Rated active power	P^*	10 kW
Rated reactive power	Q^*	2kvar
Load reactive power	P_{L1}, P_{L2}, P_{L3}, P_{L4}	10 kW
Control Parameters		
VSG1		
Power filter time constant	τ	1/60
Droop Damp coefficient	D_1,	500
Initial inertia coefficient	J_1	400
Q-V droop coefficient	n_1	0.001
VSG2		
Power filter time constant	τ	1/60
Droop Damp coefficient	D_2	900
Initial inertia coefficient	J_2	150
Q-V droop coefficient	n_2	0.001
VSG3		
Power filter time constant	τ	1/60
Droop Damp coefficient	D_3	900
Initial inertia coefficient	J_3	250
Q-V droop coefficient	n_3	0.001
VSG4		
Power filter time constant	τ	1/60
Droop Damp coefficient	D_4	500
Initial inertia coefficient	J_4	800
Q-V droop coefficient	n_4	0.001

multi-VSG system is shown in Fig. 4 and system parameter values are listed in Table 2 in Appendix A.

4.1. Comparisons with constant inertia control

Fig. 4 shows a power system with four VSGs. It is assumed that the load fluctuates at $t = 1\ s$ and $t = 4\ s$. Fig. 5(a) and (b) show the output power and the frequency of the system, respectively. The constant inertia coefficient is designed as $J_{1,2,3,4} = 400$, $J_2 = 150$, $J_3 = 250$ and $J_4 = 800$. Obviously, the waveforms indicate that serious power oscillation and undesired frequency dynamic response performance occurs with conventional VSG control after load fluctuation. Unlike SGs, the inverter-based VSG with low overcurrent capability are more susceptible to damage owing to active power oscillation. Moreover, the poor frequency dynamic response performance, such as high rate of change of frequency (RoCoF) and large frequency deviation, will result in undesirable load-shedding or massive blackouts [39–41].

To verify the validity of the proposed control, two different distributed communication topologies as shown in Fig. 6 are adopted. Fig. 7 and Fig. 8 shows the output active power, the system frequency and the variation trend of total inertia coefficient under different communication topology. Actually, it is obvious that choosing different neighbors has little impact on the performance on the adaptive inertia that can be ignored by comparing Fig. 7 with Fig. 8. The proposed distributed adaptive control strategy can suppress power oscillation and improve frequency performance in any distributed communication topology with at least one spanning tree [41,42]. In addition, the topology is chosen such that in case of any link failure the remaining network still contains at least one spanning tree. This redundancy is required to ensure link-failure resiliency. Neighbors are chosen based on economic factors in this paper. Two VSGs that are geographically close to each other are neighbors.

Since different communication topology has little impact on the system performance, here, the performance with the proposed method under communication topology (a) is mainly discussed. Fig. 7(a) and (b) present the output active power and the frequency of the system after applying the adaptive virtual inertia control where the adaptive coefficient is set as $k_1 = k_2 = k_3 = k_4 = 1000$. Fig. 7(c) shows the variation waveform of the virtual inertia coefficient after load fluctuation. In Fig. 5(a), the instantaneous impact power of VSG4 is 1400 W with conventional VSG control. It is larger compared with the instantaneous impact power 800 W in Fig. 7(a). It is evident that the impact active power is reduced in Fig. 7(a) which is more friendly to power electronic inverters and the power oscillation is suppressed between each VSG. Besides, the frequency dynamic response performance is greatly improved as shown in Fig. 7(b) that helps enhance the frequency stability of the system. At the moment of a sudden change in frequency, we can see from Fig. 7(c) that the variation trend of the virtual inertia coefficient is favorable for each frequency to approach each other. To be specific, a VSG with a relatively high initial inertia coefficient decreases inertia, and a VSG with a relatively low initial inertia increases inertia. The inertial compensation term is obtained by comparing its own frequency with adjacent frequencies in real-time. It is worth noting that the inertia coefficient goes back to its initial value at a steady state.

4.2. Comparison with different inertia coefficients

In order to investigate the influence of the key control parameter on system performance, i.e. inertia compensation coefficient k_i, a set of different k_i values (0, 200, 500, 1000, 2000) are applied in the proposed control method. In order to clearly see the variation of system output power and frequency waveform with the change of k_i, the waveform of VSG3 is listed in this part to illustrate the effectiveness of the control strategy. As shown in Fig. 9(a), the output active powers oscillation has been effectively suppressed. Additionally, with the increase of the inertia compensation coefficient k_i, the power oscillation suppression effect is better. At the same time, the maximum frequency deviation and maximum RoCoF has been reduced as shown in Fig. 9(b). In other words, the frequency dynamic response performance has been greatly improved. Besides, it takes less time to reach steady state. Conventionally, the inertia coefficient is designed to slow down the RoCoF. It is worth mentioning that the proposed adaptive inertia is designed to suppress the frequency oscillation and does not change the general trend of frequency change. The variation trend of the total inertia coefficient with different adaptive virtual inertia coefficient (k_i) is shown in Fig. 9 (c). With larger k_i, the range of inertia will increase in the transient process. Thus, a better effect of oscillation suppression can be obtained.

4.3. Damping performance under short-circuit fault

In this case, it is assumed that a three-phase short circuit on transmission Line 2, near VSG1 occurs at t = 1 s and is cleared at t = 1.1 s. In order to better observe the damping ability of the proposed control strategy, the output active powers and system frequency of VSG1 with conventional VSG control and proposed adaptive virtual inertia control are presented in Fig. 10. It is obvious that the proposed method has a good damping performance on power and frequency oscillations. Besides, the maximum frequency deviation is reduced to a large extent and the system adjustment time is also reduced.

4.4. Robustness performance under noises

To test the robustness performances of proposed control, high-frequency noise is imposed on the detection of the system operating frequency. Fig. 11(a) and (b) show the frequency without and with adaptive virtual inertia control, respectively. Apparently, even though high-frequency noise exists in the system frequency detection, the proposed control method also helps improve frequency dynamic response, and thus suppress power oscillation. Obviously, the proposed method is not sensitive to high-frequency noises.

4.5. Communication delay analysis

This section analyzes the impact of transmission latency on the system performance of the proposed method, which is critically important. Since the control strategy proposed in this paper relies on distributed communication, i.e. the information interaction between VSG neighbors. Fig. 12 (a) and (b) show the output active power and the frequency response waveform of VSG3 in the system under different delay times with $k_i = 1000$. In the absence of communication delay, the adaptive inertia does not change the overall trend in the frequency and only helps suppress the frequency oscillation. As the communication delay increases, the overall RoCoF of the system decreases. Thus, the dynamic response performance is still improved. Moreover, it is obvious that the power oscillation is effectively suppressed even in the presence of communication delay and the range of permissible communication delays is wide as shown in Fig. 12. It should be noted that depending on the purpose of using the controller, the allowable latency is different. To improve stability and state estimation accuracy of the electrical networks, the latency of about 100 ms is acceptable, which is well-suited for today's technologies even for large networks [43,44]. Therefore, in the proposed control method, with the low amount of information and especially simple calculations, the delay time can easily be implemented in<100 ms. Consequently, the effectiveness of the proposed control strategy is verified within the allowable delay range.

4.6. Communication failure analysis

In this case, the performance of the proposed distributed control strategy is tested in the case of a single communication link failure. The latency time due to the communication delay is set to be $T_d = 80$ ms and the adaptive inertia coefficient is set to be $k_i = 1000$. It is assumed that

load fluctuates at t = 1 s and t = 4 s and a link failure occurs between VSG2 and VSG3. Fig. 13(a) and (b) shows the output active power and the system frequency of VSGs. Compared with Fig. 5 where $k_i = 0$, it is obvious that the power oscillation of the system is suppressed and frequency dynamic response is improved even in the case of single line communication failure. Compared with Fig. 7 without link failure, it is apparent that the more information obtained, the better the effect of power oscillation suppression. In addition, increasing the adaptive coefficient is also an important means to improve the suppression effect of power oscillation.

4.7. Performance under nonlinear load

In this case, the performance of the proposed distributed control strategy is tested under nonlinear load. The P_L as shown in Fig. 4 is replaced by an uncontrolled rectifier bridge. Fig. 14(a) shows the FFT analysis of load voltage, the THD of which has reached 5.12%. Fig. 14(b) and (c) present the output active power and the frequency of the system with the adaptive virtual inertia control. It is obvious that the power oscillation of the system is suppressed and frequency dynamic response is improved. Thus, the effectiveness of the proposed method has been verified under harmonic load.

5. Hardware-In-Loop (HIL) results

In this section, the proposed adaptive virtual inertia control is verified by real-time HIL test based OPAL-RT (OP4510). The structure of four-VSG grid shown in Fig. 4 has been studied.

5.1. Case1: Conventional VSG control method

Fig. 15(a) and 15(b) show the output power and the frequency of the system under load fluctuation, respectively. The constant inertia coefficient is designed as $J_{1,2,3,4} = 400$, $J_2 = 150$, $J_3 = 250$ and $J_4 = 800$. It should be noted that we set $f_i^{'} = (f_i - 50)$ Hz in order to better observe the dynamic process of frequency clearly as shown in Fig. 15(b). With conventional VSG control, the power oscillation of the system can be observed in Fig. 15(a) when load fluctuates, and the instantaneous impact power is very large. Besides, the frequency oscillation phenomenon is also obvious which results in large frequency deviation.

5.2. Case2: Proposed VSG control method

With the proposed adaptive virtual inertia control method (k_i = 1000), the improved output active power, the frequency of the system and the variation trend of total inertia coefficient are shown in Fig. 16. It is evident that the impact active power is reduced in Fig. 16(a) which is more friendly to power electronic inverters and the power oscillation is suppressed between each VSG. Obviously, the proposed method has smaller impact current during post-contingency dynamics which is desirable for a converter [40,45]. The maximum frequency deviation and the maximum RoCoF has been reduced as shown in Fig. 16(b). In other words, the frequency dynamic response performance has been greatly improved. The hardware-in-loop results are consistent with the simulation results compared with Fig. 5 and Fig. 7.

5.3. Case3: Proposed VSG control method under time delay

This case verifies the effectiveness of the proposed adaptive virtual inertia control method under time delay. The delay time is set as 100 ms, which is acceptable and well-suited for large networks [43,44]. Fig. 17 (a) and (b) show the output active power and the frequency response waveform with $k_i = 1000$. Obviously, even in the case of communication delays, the impact active power is reduced which is more friendly to power electronic inverters and the power oscillation is suppressed between each VSG. Besides, the frequency dynamic response performance is greatly improved that helps enhance the frequency stability of the system.

6. Conclusion

This study introduces an adaptive virtual inertia control method for stability enhancement of a multi-VSG grid. The advantages of the proposed control method include: (1) The proposed method contributes to power oscillation suppression and dynamic frequency response improvement in the multi-VSG grid. (2) It is a practical control algorithm that avoid the direct frequency derivative action which introduces high-frequency noise. Moreover, it has good robustness performance even under noise. (3) The proposed method has a high communication delay margin and can still operate stably under a large communication delay. Besides, it is not susceptible to any single link failure, which leads to a more reliable control framework. The effectiveness of the proposed method has been verified by simulation results and HIL results.

Declaration of Competing Interest

The authors declare that they have no known competing financial interests or personal relationships that could have appeared to influence the work reported in this paper.

Acknowledgements

This work was supported by the science and technology innovation Program of Hunan Province under Grant 2020RC4002, the Project of Innovation-driven Plan in Central South University under Grant 2019CX003, the National Natural Science Foundation of China under Grants 61933011, and the Fundamental Research Funds for the Central Universities of Central South University under Grant 2020zzts578.

Appendix A

See Table 2.

References

[1] Rocabert J, Luna A, Blaabjerg F, Rodriguez P. Control of Power Converters in AC Microgrids. IEEE Trans Power Electron Nov 2012;27(11):4734–49.
[2] Kryonidis GC, Kontis EO, Chrysochos AI, Oureilidis KO, Demoulias CS, Papagiannis GK. Power Flow of Islanded AC Microgrids: Revisited. IEEE Trans Smart Grid Jul 2018;9(4):3903–5.
[3] Zhong Q-C. Virtual Synchronous Machines: A unified interface for grid integration. IEEE Power Electron Mag 2016;3(4):18–27.
[4] Eftekharnejad S, Vittal V, Heydt GT, Keel B, Loehr J. Small Signal Stability Assessment of Power Systems With Increased Penetration of Photovoltaic Generation: A Case Study. IEEE Trans Sustainable Energy 2013;4(4):960–7.
[5] Delille G, Francois B, Malarange G. Dynamic Frequency Control Support by Energy Storage to Reduce the Impact of Wind and Solar Generation on Isolated Power System's Inertia. IEEE Trans Sustainable Energy 2012;3(4):931–9.
[6] Sullivan JO, Rogers A, Flynn D, Smith P, Mullane A, Malley MO. Studying the Maximum Instantaneous Non-Synchronous Generation in an Island System—Frequency Stability Challenges in Ireland. IEEE Trans Power Syst 2014;29 (6):2943–51.
[7] Ruttledge L, Miller NW, O'Sullivan J, Flynn D. Frequency Response of Power Systems With Variable Speed Wind Turbines. IEEE Trans Sustainable Energy 2012; 3(4):683–91.
[8] P. Kundur, "Power System Stability and Control," The EPRI Power system Engineering Series.
[9] W. Uijlings, D. Street, and S. London, "An independent analysis on the ability of Generators to ride through Rate of Change of Frequency values up to 2Hz/s.".
[10] Zhong Q, Weiss G. Synchronverters: Inverters That Mimic Synchronous Generators. IEEE Trans Ind Electron 2011;58(4):1259–67.
[11] Dreidy M, Mokhlis H, Mekhilef S. Inertia response and frequency control techniques for renewable energy sources: A review. Renew Sustain Energy Rev 2017;69:144–55.
[12] Bevrani H, Ise T, Miura Y. Virtual synchronous generators: A survey and new perspectives. Int J Electr Power Energy Syst 2014;54:244–54.
[13] Pulendran S, Tate JE. Energy Storage System Control for Prevention of Transient Under-Frequency Load Shedding. IEEE Trans Smart Grid Mar 2017;8(2):927–36.

[14] Koohi-Kamali S, Tyagi VV, Rahim NA, Panwar NL, Mokhlis H. Emergence of energy storage technologies as the solution for reliable operation of smart power systems: A review. Renew Sustain Energy Rev 2013;25:135–65.
[15] Zhong Q-C. Power-Electronics-Enabled Autonomous Power Systems: Architecture and Technical Routes. IEEE Trans Ind Electron Jul 2017;64(7):5907–18.
[16] M. Kezunovic, V. Vittal, S. Meliopoulos, and T. Mount, "The Big Picture Smart Research for Large-Scale Integrated Smart Grid Solutions," IEEE Power & Energy Magazine, vol. 10, no. 4, pp. 22-34, Jul-Aug 2012.
[17] Roldan-Perez J, Rodriguez-Cabero A, Prodanovic M. Design and Analysis of Virtual Synchronous Machines in Inductive and Resistive Weak Grids. IEEE Trans Energy Convers Dec 2019;34(4):1818–28.
[18] Shi K, Song W, Ge H, Xu P, Yang Y, Blaabjerg F. Transient Analysis of Microgrids With Parallel Synchronous Generators and Virtual Synchronous Generators. IEEE Trans Energy Convers 2020;35(1):95–105.
[19] Dong S, Chen YC. Adjusting Synchronverter Dynamic Response Speed via Damping Correction Loop. IEEE Trans Energy Convers 2017;32(2):608–19.
[20] Shintai T, Miura Y, Ise T. Oscillation Damping of a Distributed Generator Using a Virtual Synchronous Generator. IEEE Trans Power Delivery 2014;29(2):668–76.
[21] Zheng T, Chen L, Wang R, Li C, Mei S. Adaptive damping control strategy of virtual synchronous generator for frequency oscillation suppression. In: *12th IET International Conference on AC and DC Power Transmission (ACDC 2016)*; 2016,. p. 1–5.
[22] Huang L, Xin H, Wang Z. Damping Low-Frequency Oscillations Through VSC-HVdc Stations Operated as Virtual Synchronous Machines. IEEE Trans Power Electron 2019;34(6):5803–18.
[23] Alipoor J, Miura Y, Ise T. Power System Stabilization Using Virtual Synchronous Generator With Alternating Moment of Inertia. IEEE Journal of Emerging and Selected Topics in Power Electronics 2015;3(2):451–8.
[24] X. Ningyi, W. Yue, L. Mingxuan, W. Wenti, W. Ning, and L. Jiliang, "An optimal control method of virtual angular acceleration to improve transient response based on virtual synchronous generator," in 2017 IEEE 3rd International Future Energy Electronics Conference and ECCE Asia (IFEEC 2017 - ECCE Asia), 2017, pp. 1559-1563.
[25] Karimi A, et al. Inertia Response Improvement in AC Microgrids: A Fuzzy-Based Virtual Synchronous Generator Control. IEEE Trans Power Electron 2020;35(4):4321–31.
[26] Hou X, Sun Y, Zhang X, Lu J, Wang P, Guerrero JM. Improvement of Frequency Regulation in VSG-Based AC Microgrid Via Adaptive Virtual Inertia. IEEE Trans Power Electron 2020;35(2):1589–602.
[27] Cheng C, Yang H, Zeng Z, Tang S, Zhao R. Rotor inertia adaptive control method of VSG. Automation of Electric Power Systems 2015;39(19):82–9.
[28] Alipoor J, Miura Y, Ise T. Stability Assessment and Optimization Methods for Microgrid With Multiple VSG Units. IEEE Trans Smart Grid 2018;9(2):1462–71.
[29] Wang W, Jiang L, Cao Y, Li Y. A Parameter Alternating VSG Controller of VSC-MTDC Systems for Low Frequency Oscillation Damping. IEEE Trans Power Syst 2020;35(6):4609–21.
[30] Rosso R, Engelken S, Liserre M. Robust Stability Analysis of Synchronverters Operating in Parallel. IEEE Trans Power Electron 2019;34(11):11309–19.
[31] Cheng C, Zeng Z, Yang H, Zhao R. "Wireless parallel control of three-phase inverters based on virtual synchronous generator theory," in. International Conference on Electrical Machines and Systems (ICEMS) 2013;2013:162–6.
[32] Liu J, Miura Y, Bevrani H, Ise T. Enhanced Virtual Synchronous Generator Control for Parallel Inverters in Microgrids. IEEE Trans Smart Grid 2017;8(5):2268–77.
[33] Shuai Z, Huang W, Shen ZJ, Luo A, Tian Z. Active Power Oscillation and Suppression Techniques Between Two Parallel Synchronverters During Load Fluctuations. IEEE Trans Power Electron 2020;35(4):4127–42.
[34] Mao M, Qian C, Ding Y. Decentralized coordination power control for islanding microgrid based on PV/BES-VSG. CPSS Transactions on Power Electronics and Applications 2018;3(1):14–24.
[35] Choopani M, Hosseinain SH, Vahidi B. A novel comprehensive method to enhance stability of multi-VSG grids. Int J Electr Power Energy Syst 2019;104:502–14.
[36] Choopani Mahdi, Hosseinian Seyed Hossein, Vahidi Behrooz. New Transient Stability and LVRT Improvement of Multi-VSG Grids Using the Frequency of the Center of Inertia. IEEE Trans Power Syst 2020;35(1):527–38.
[37] Machowski J, Lubosny Z, Bialek JW, Bumby JR. Power system dynamics: stability and control. John Wiley & Sons; 2020.
[38] Meyer CD. Matrix analysis and applied linear algebra. Siam 2000.
[39] Debry M-S, Denis G, Prevost T, Xavier F, Menze A. Maximizing the penetration of inverter-based generation on large transmission systems: the migrate project. in *6th Solar Integration Workshop*. 2017.
[40] Milano F, Dörfler F, Hug G, Hill DJ, Verbič G. "Foundations and Challenges of Low-Inertia Systems (Invited Paper)," in. Power Systems Computation Conference (PSCC) 2018;2018:1–25.
[41] Nasirian Vahidreza, Davoudi Ali, Lewis Frank L, Guerrero Josep M. Distributed Adaptive Droop Control for DC Distribution Systems. IEEE Trans Energy Convers 2014;29(4):944–56.
[42] Nasirian V, Moayedi S, Davoudi A, Lewis FL. Distributed Cooperative Control of DC Microgrids. IEEE Trans Power Electron 2015;30(4):2288–303.
[43] Arani MFM, Mohamed YAI, El-Saadany EF. Analysis and Mitigation of the Impacts of Asymmetrical Virtual Inertia. IEEE Trans Power Syst 2014;29(6):2862–74.
[44] Chai WK, et al. An Information-Centric Communication Infrastructure for Real-Time State Estimation of Active Distribution Networks. IEEE Trans Smart Grid 2015;6(4):2134–46.
[45] Huang Linbin, Xin Huanhai, Wang Zhen, Zhang Leiqi, Wu Kuayu, Hu Jiabing. Transient Stability Analysis and Control Design of Droop-Controlled Voltage Source Converters Considering Current Limitation. IEEE Trans Smart Grid 2019;10 (1):578–91.